Published in final edited form as:
J Magn Reson Imaging. 2008 July ; 28(1): 236–241. doi:10.1002/jmri.21425.

3T MR With Diffusion Tensor Imaging and Single-Voxel Spectroscopy in Giant Axonal Neuropathy

Christiana Brenner, MD[1,*], **Carlos Eduardo Speck-Martins, MD, PhD**[2], **Luciano Farage, MD**[2], and **Peter B. Barker, DPhil**[3]

[1] The Hospital for Sick Children, Diagnostic Imaging Department, Toronto, Ontario, Canada [2] Rede Sarah de Hospitais, Department of Clinical Genetics, Brasilia, Brazil [3] Johns Hopkins University School of Medicine, Department of Radiology, Baltimore, Maryland

Abstract

Magnetic resonance imaging (MRI), diffusion tensor imaging (DTI), and MR spectroscopy (MRS) data were obtained in a patient with giant axonal neuropathy (GAN) and compared to a control group. Fractional anisotropy (FA) and apparent coefficient diffusion (ADC) data were obtained from specific white matter tracts including the corticospinal tracts (CST), corpus callosum (CC), optic radiations (OR), and middle cerebellar peduncle (MCP). Analysis of the MRS was performed. DTI parameters and MRS results were correlated with the neuropathological findings described for GAN. No significant difference between the FA of the CC of the patient and the control group was found. However, there was a significant difference between the FA of the CST, OR, and MCP of the patient and the control group. The ADC values for all tracts of the patient were significantly increased. N-acetylaspartate to creatine (NAA/Cr) and N-acetylaspartate to choline (NAA-Cho) (choline) metabolite ratios were slightly decreased and choline to creatine (Cho/Cr) and myoinositol to creatine (Ins/Cr) metabolite ratios were increased in the parietal gray and white matter of the patient as compared to the control group. Cerebellar involvement was less evident. The DTI and MRS findings suggest myelin and axonal damage.

Keywords

leukoencephalopathy; MRI; MR spectroscopy; diffusion tensor imaging

Giant axonal neuropathy (GAN) is a rare, autosomal recessive neurodegenerative disorder that affects the peripheral and central nervous system. The GAN1 gene has been mapped to chromosome 16q24.1 and encodes a ubiquitous protein named Gigaxonin (1).

Peripheral nerve biopsy shows giant axonal swelling due to accumulation of neurofilaments, the primary intermediate filament in neurons. Gigaxonin interacts with MAP1B, a microtubule (MT) associated protein involved in maintaining the integrity of the cytoskeleton structure and promoting neuronal stability.

Patients present with normal or delayed early development followed by progressive weakness and gait disturbance. They usually become wheelchair-dependent and die between 10 and 30

[*]Address reprint requests to: C.B., the Hospital for Sick Children, Diagnostic Imaging Department, 555 University Ave., Toronto, ON M5G 1X8, Canada. chrisbre7166@hotmail.com.

The data in this article were collected at Rede Sarah de Hospitais, Brasilia, Brazil.

years of age (2). Neurophysiology studies display abnormalities in auditory, somatosensory, and visual evoked potentials (3); electromyography demonstrates axonal peripheral neuropathy (2,4,5). Brain magnetic resonance imaging (MRI) findings are variable. Cerebellar and cerebral central white matter is usually affected. Other structures involved are the posterior limb of internal capsule, pyramidal tracts, medial lemniscus, cerebellar peduncle, and the hilus of the dentate nucleus (6).

In this report, the clinical, neurophysiological, and MRI findings of a male with GAN are described. Magnetic resonance spectroscopy (MRS), fractional anisotropy (FA), and apparent diffusion coefficient (ADC) values data measured from the diffusion tensor imaging (DTI) were obtained in selected regions and compared with a control group.

CASE REPORT

The patient was a 12-year-old male with unremarkable family and prenatal history. His parents were healthy and first-degree cousins. His motor and cognitive milestones were normal. Gait disturbance and falls started at 3 years of age, followed by foot deformity, distal inferior limbs atrophy, scoliosis, and decreased visual acuity. At 5 years of age dysarthria and uncoordinated hand movements were noticed. At 11 years of age he became dependent on a walking frame. His school performance was initially normal, but he has recently had difficulties due to visual loss. On examination, he showed macrocranium, bilateral optic nerve atrophy and ptosis, and facial weakness. No ocular paralysis or nystagmus was observed. His speech, arm movements, and gait were severely ataxic, with bilateral rebound phenomenon. Distal limb paresis was noted, most markedly affecting foot dorsiflexion and inversion. Distal vibration sensory loss was noticed. Tendon reflexes were absent and bilateral Babinski's sign was observed. Equinovarus talipes and kyphoscoliosis were present.

Neurophysiology studies were performed on two occasions 4 years apart. Auditory, somatosensory, and visual evoked potentials were normal at 7 years of age. At 11 years of age only wave I was seen on auditory evoked potentials. There was absence of peripheral and central responses on somatosensory evoked potentials, and absence of responses on reverse pattern and flash visual evoked potentials. Electromyography was normal at 7 years of age. Four years later signs of a severe axonal sensory and motor neuropathy were found, with absence of sensory and motor nerve action potentials in the lower limbs and reduced compound muscular action potentials amplitudes in the upper limbs. Electromyography displayed a generalized neurogenic pattern.

A neuropathological diagnosis of GAN was obtained by sural nerve biopsy which demonstrated giant axons containing a large quantity of neurofilaments and neurotubules.

MATERIALS AND METHODS

Routine brain and spinal MRI including axial, sagittal, and coronal T2-weighted images (T2WI) and axial T1-weighted images (T1WI) were obtained on a 1.5T scanner (Siemens Magneton Symphony, Erlangen, Germany). Axial, sagittal, and coronal (T2WI), proton MRS and DTI were acquired on a 3.0T scanner (Siemens Trio). MRS was acquired with a single-voxel stimulated echo acquisition mode localization sequence (TR/TE = 2000/30) on an 8-channel head coil. DTI data were acquired in about 3 minutes using an echo-planar sequence with 12 gradients directions, with b-values of 0 and 1000s/mm^2, TR 4500 msec, TE 100 msec, 3 NEX, field of view (FOV) = 223 mm, matrix 192 × 192, slice thickness = 2.5 mm, with 70% gap.

Five healthy volunteers (age range 10–16 years old, two females and three males) comprised the control group for MRS, FA, and ADC analysis. Previous reports have shown no sex

differences (7) and little variation in metabolites and DTI parameters in this age range (8,9). All examinations were performed with the written consent of parents. None of the subjects had a history of psychiatric or neurological disorders, and none had intracranial pathologic lesions revealed by the T2WI obtained. No sedation was necessary for any subject.

The 8 cm^3 MRS voxels were selected from T2WI and were located in the right parieto-occipital white matter, parietal gray matter, right cerebellar white matter, and left cerebellar gray matter.

The corticospinal tracts (CST), optic radiations (OR), middle cerebellar peduncle (MCP), and corpus callosum (CC) tracts were identified in the FA color, low b, and FA maps, as well as in the T2W images. The FA and ADC values were obtained from the regions of interest (ROIs). The ROIs were drawn for 20 brain structures, from the medula ablongata to the centrum semiovale covering the CST. Seven ROIs were obtained for the OR. Three ROIs were drawn covering the MCP. For the CC seven ROIs were obtained. The ROIs varied in shape and size to fit the structure of interest. Tractography was performed to check for spurious data (crossing fibers). The ROIs were manually drawn by one radiologist in the scan console (C.B.).

The software supplied by the manufacturer was used to measure MRS peak area integrals and metabolite ratios were expressed relative to creatine (Cr). The following metabolite ratios were calculated: N-acetylaspartate (NAA/Cr), choline (Cho/Cr), myoinositol (Ins/ Cr), and NAA/ Cho. The mean and standard deviation (SD) of the patient and the control group integrals values and metabolite ratios were calculated.

The FA and ADC values obtained for each specific tract for the control group and patient were grouped. A descriptive analysis was performed to assess differences between the controls and patient. In addition, a Bonferroni correction for multiple comparisons was applied. A nonparametric statistical method, Mann–Whitney test, was used to assess differences in FA and ADC values between the control group and the patient for each different tract. The level of significance in all tests was set to $P < 0.05$. The software used was SPSS 14.0 (Chicago, IL).

RESULTS

The patient's routine images displayed spinal cord atrophy with involvement of the posterior column in the cervical segment. In the medulla oblongata, there were bilateral and symmetrical, T2WI hyperintense lesions in the inferior olivary, gracile and cuneate nuclei, and anterior and posterior spinocerebellar tracts. In the posterior fossa there was involvement of the inferior and middle cerebellar peduncles. In the pons, transverse fibers were involved. In the midbrain, cortical spinal tracts, medial lemniscus, and periaqueductal gray substance were compromised. Cerebellar white matter was diffusely hyperintense. Severe optic tract atrophy was observed. The medial nuclei of the thalamus, posterior crus of the internal capsule, extreme capsule, deep and periventricular white matter were affected. The corpus callosum was slightly thin. Subcortical U-fibers were spared. Note was made of the presence of a *cavum septum pellucidum* and *vergae*. There was slight enlargement of the ventricles.

MRS displayed mildly reduced NAA/Cr ratios in all regions, except for the cerebellar gray matter, and strongly increased Cho/Cr ratio in all regions but cerebellar white matter. An increased Ins/Cr ratio was also found in all regions studied. NAA/Cho was decreased in all brain regions studied in the patient compared to controls (Table 1). Integral values for NAA, Cr, and Cho were overall decreased and myoinositol was generally increased (Table 2; Fig. 1).

There was no statistical difference between the FA and ADC means, compared two by two, between the control group and patient in the Bonferroni multiple comparisons. The level of significance was set to $P < 0.05$.

Fractional anisotropy was significantly decreased in the CST, OR, and MCP ($P < 0.05$). In the corpus callosum, FA was not different from the control group (Table 3). ADC values were increased in all tracts ($P < 0.05$) (Table 4).

DISCUSSION

GAN is a very rare degenerative disease. Around 70 cases have been reported and its physiopathology is unclear. The discovery of gigaxonin suggests a relationship with abnormal axonal transport. GAN appears to be a heterogeneous disease both clinically and radiologically. The earliest presentation is with peripheral nervous system (PNS) involvement and thereafter there is a progressive sensory-motor axonal neuropathy with variable cranial nerve involvement. The progression is inconsistent and there have been cases with a relatively benign course of disease (2). The reported imaging findings on MR in GAN include involvement of cerebellar and cerebral white matter with sparing of the subcortical U-fibers, a variable degree of cerebral atrophy, and thinning of the corpus callosum (4,5,10). The other findings include the persistence of *cavum sepum pellucium* and *vergae* and involvement of the posterior *crus* of internal capsule and thalamus (11).

Histopathological findings are enlarged axons with accumulation of neurofilaments, astrocytic degeneration, demyelination, and the presence of Rosenthal fibers. Because axonal transport is impaired, the early presentation of GAN is a distal axonopathy, most severely affecting the peripheral nerves, posterior columns, cerebellum, and pyramidal tracts (12,13).

The major detectable brain metabolites include the predominantly neuroaxonal compound NAA, the energy metabolites creatine and creatine phosphocreatine (Cr), Cho compounds involved in membrane turnover, and the possible glial (astrocytic) marker, and brain osmolyte myoinositol (Ins) (10). There are only two previous studies about cerebral proton MRS in GAN (10–14). Their findings were not completely in accordance, which could in part be explained by different methodology and/or different stages of disease progression. The study by Alkan et al (14) found normal NAA/Cr ratios, and increased Cho/Cr and Ins/Cr ratios in affected frontal and parietal white matter, while the study by Brockmann et al (10) found decreased NAA, as well as increased Cho, Cr, and lactate (Lac) in white matter, as well as increased Cho and Ins in white matter. Brockman et al (10) report a high-quality study performed at 2.0T using the LC Model for metabolite quantification. In both cases the spectroscopic findings (increased Cho and Ins) were interpreted as demyelination and glial proliferation, while (in the Brockmann study) decreased NAA was interpreted as axonal loss.

In the current study the metabolite ratios relative to Cr and the integrals values were used, since methods for estimating metabolite concentrations were unavailable. The metabolites peak area reflects the metabolite concentration. The estimate concentration was obtained from the peak integration (integrals) performed by the scanner software. Although the use of integrals values presents limitations (15), the analysis of this metabolite concentration was used to suggest an explanation for the metabolite ratio findings (Tables 1, 2). In keeping with other reports, we found a large increase in Cho/Cr and Ins/Cr ratios in nearly all brain regions covered. The NAA/Cr ratio was mildly decreased in the patient compared to controls, as well as the NAA/Cho ratio. This could be secondary to a decrease in the NAA or increase in Cho. The integrals analysis showed decreased NAA and Cr as well as Cho.

Based on the analysis of the metabolite ratios we are in accordance with Alkan et al and Brockman et al regarding the presence of demyelination and glial proliferation. Although we do not have the metabolite quantification, our findings of low NAA/Cr and NAA/Cho suggests axonal damage, in accordance with Brockman et al's study.

Information on tissue microstructure and architecture for each voxel can be obtained from diffusion data acquired by DTI. The mean diffusivity characterizes the overall mean-squared molecular displacement (average ellipsoid size) (16). Fractional anisotropy (FA) is a rotational invariant index of anisotropic diffusion defined by the principle three eigenvalues of the brain water diffusion ellipsoid. The principal eigenvector is considered parallel to the direction of the axons. Low FA values suggest that there is a mixture of fibers running in different directions, loss of axonal bundles, or impaired water diffusion along the axons (17). A recent review summarizes the relationship between MR measurements of water diffusion and its anisotropy with the underlying microstructure of neural fibers (18). It was concluded that the main determinant of anisotropy in nervous tissue is the presence of intact cell membranes and myelination serves to modulate anisotropy (18).

The diffusion coefficient is a physical parameter that directly reflects the physical properties of the tissues in terms of the random translational movement of the molecules (16). Studies of cerebral white matter development in human neonates have shown a decrease in the mean diffusivity and an increase in the degree of anisotropy with maturation (18). These diffusion changes are linked to the increase in myelination, reduction in brain water, greater cohesiveness and compactness of the fibers tracts, and the reduced extra-axonal space (greater packing) as the white matter matures over time (18). In GAN there are marked cytoskeletal abnormalities with impaired axonal transport and axonal distension with accumulation of neurofilaments. This leads to axonal degeneration and neuronal death (6). Because the myelin sheath and the axons are mutually dependent, demyelination also occurs, with gliosis as the final event. In GAN, increased intracellular water secondary to axonal distension and decreased myelin leads to increased mean diffusivity and decreased FA. As far as we are aware, DTI has not been previously reported in GAN. The low FA values observed in the current case also suggests axonal loss in the OR, MCP, and CST in accordance with pathology data (11,12). Our data are also in accordance with the observation of low NAA/Cr and low NAA/Cho (suggestive of axonal loss) in white matter regions. There was no significant difference in FA between the patient and the control group in the corpus callosum. Nevertheless, ADC values were increased in this structure as well as in all the other tracts. Gulani et al (19) measured the anisotropy and ADC values in an X-linked recessive Wistar rat mutant that shows near total lack of myelination in its central nervous system and compared it to a control group. They found an ≈20% decrease in anisotropy and ≈50% increase in mean diffusivity. They concluded that residual structures, namely, the membranes of the numerous axons, were sufficient for significant anisotropic diffusion in the model but the absence of myelin altered the absolute ADC values. The lack of myelin increased water mobility in the perpendicular direction (18). Based on this observation, we hypothesize that, in our patient, there was decreased myelin in the CC with relative preservation of axonal membranes. This is compatible with the relative sparing of the CC seen on conventional T2-weighted images.

In conclusion, GAN is a chronic disease with clinical and genetic heterogeneity as previously described. Data about MRS in GAN is scarce, and there have been no prior DTI observations. The results of this combined MRS and DTI case study suggest that at the time the patient was imaged there was demyelination, axonal damage, and glial proliferation in the white matter. Mild axonal loss in the gray matter and relative preservation of the integrity of the fibers of the corpus callosum was present. These advanced MR techniques may therefore complement conventional MRI in monitoring and quantifying CNS involvement in GAN.

Acknowledgments

The authors wish to thank Dr. Emma Helm for revising the manuscript.

References

1. Bruno C, Bertini E, Frederico A, et al. Clinical and molecular findings in patients with giant axonal neuropathy (GAN). Neurology 2004;62:13–16. [PubMed: 14718689]
2. Gordon N. Giant axonal neuropathy. Dev Med Child Neurol 2004;46:717–719. [PubMed: 15473179]
3. Majnemer A, Rosenblatt B, Watters G, et al. Giant axonal neuropathy: central abnormalities demonstrated by evoked potentials. Ann Neurol 1986;19:394–396. [PubMed: 3010802]
4. Lampl Y, Eshel Y, Ben-David E, Gilad R, Sarova-Pinhas I, Sandbank U. Giant axonal neuropathy with predominant central nervous system manifestations. Dev Med Child Neurol 1992;34:164–169. [PubMed: 1310292]
5. Stollhoff K, Albani M, Goebel HH. Giant axonal neuropathy and leukodystrophy. Pediatr Neurol 1991;7:69–71. [PubMed: 2029298]
6. Marjo, S.; Van der Knaap; Jaap Valk. Giant axonal neuropathy. In: Heilmann, U., editor. Magnetic resonance of myelination and myelin disorders. 3. Heidelberg: Springer; 2005. p. 436-441.
7. Kadota T, Horinouchi T, Kuroda Chikazumi. Development and aging of the cerebrum: assessment with proton MR spectroscopy. Am J Neuroradiol 2001;22:128–135. [PubMed: 11158898]
8. Horská A, Kaufmann WE, Brant LJ, et al. In vivo quantitative proton MRSI study of brain development from childhood to adolescence. J Magn Reson Imaging 2002;15:137–143. [PubMed: 11836768]
9. Mukherjee P, McKinstry RC. Diffusion tensor imaging and tractography of human brain development. Neuroimag Clin N Am 2006;16:19–43.
10. Brockmann K, Pouwels PJW, Dechent P, et al. Cerebral proton magnetic resonance spectroscopy of a patient with giant axonal neuropathy. Brain Dev 2003;25:45–50. [PubMed: 12536033]
11. Demir E, Bomont P, Erdem S, et al. Giant axonal neuropathy: clinical and genetic study in six cases. J Neurol Neurosurg Psychiatry 2005;76:825–832. [PubMed: 15897506]
12. Kretzschmar HA, Berg BO, Davis RL. Giant axonal neuropathy. Acta Neuropathol 1987;73:138–144. [PubMed: 3604581]
13. Thomas C, Love S, Powell HC, Schultz P, et al. Giant axonal neuropathy: correlation of clinical findings with postmortem neuropathology. Ann Neurol 1987;22:79–84. [PubMed: 3631924]
14. Alkan A, Kutlu R, Sigirci A, et al. Giant axonal neuropathy: MRS findings. J Neuroimaging 2003;13:371–375. [PubMed: 14569833]
15. Ernest, T. Quantification and analysis in MR spectroscopy. In: Gillard, JH.; Waldman, AD.; Barker, PB., editors. Clinical MR neuroimaging. 1. Cambridge, UK: Cambridge University Press; 2005. p. 27-37.
16. Le Bihan D, Mangin JF, Poupon C, et al. Diffusion tensor imaging: concepts and applications. J Magn Reson Imaging 2001;13:534–546. [PubMed: 11276097]
17. Jones, DK. Fundamentals of diffusion MR imaging. In: Gillard, JH.; Waldman, AD.; Barker, PB., editors. Clinical MR neuroimaging. 1. Cambridge, UK: Cambridge University Press; 2005. p. 54-85.
18. Beaulieu C. The basis of anisotropic water diffusion in the nervous system — a technical review. NMR Biomed 2002;15:435–455. [PubMed: 12489094]
19. Gulani V, Webb AG, Duncan ID, Lauterbur PC. Apparent diffusion tensors measurements in myelin-deficient rat spinal cords. Magn Reson Med 2001;45:191–195. [PubMed: 11180424]

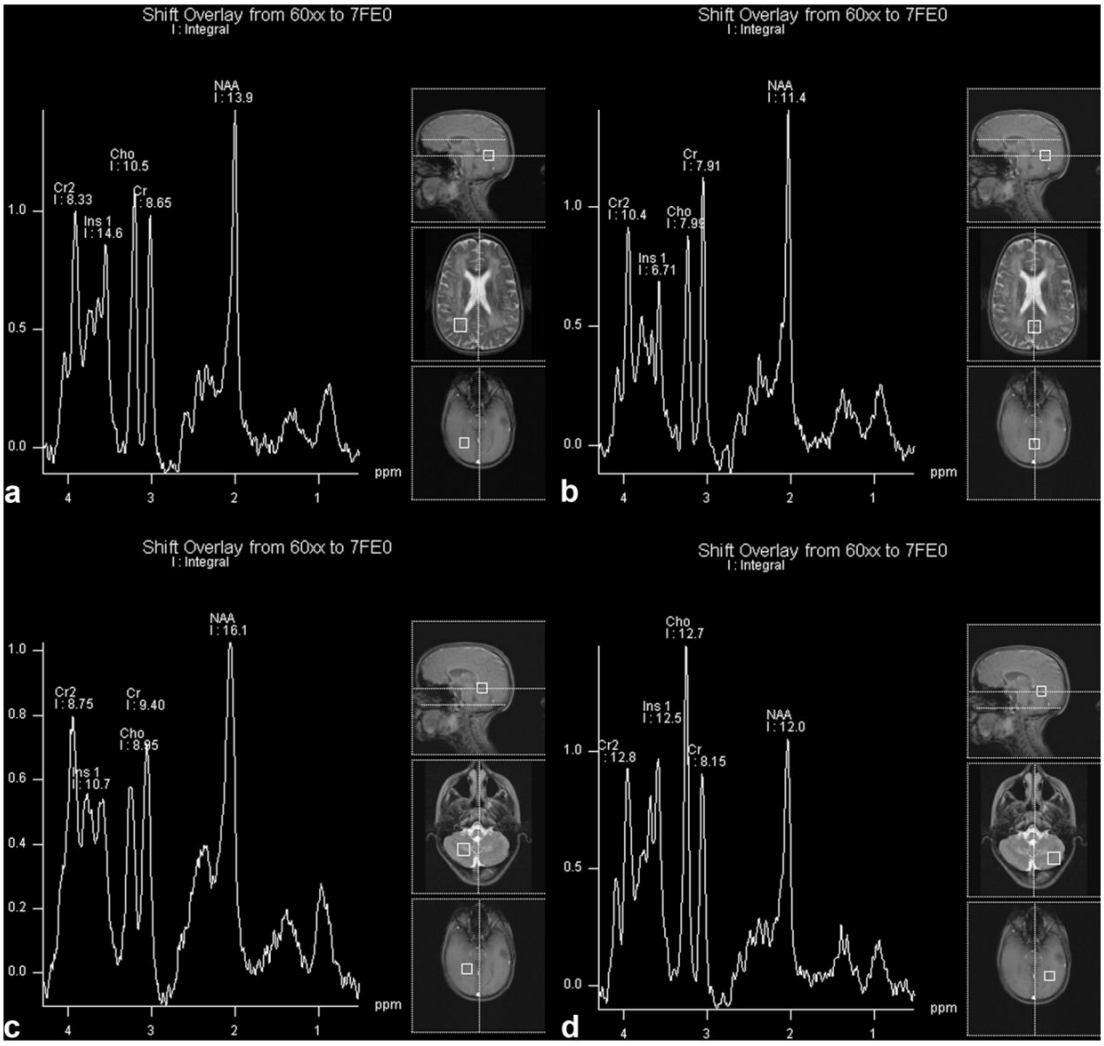

Figure 1.
The patient's spectra. PWM, parietal white matter; PGM, parietal gray matter; C, cerebral; WM, cerebellar white matter. GM, cerebellar gray matter.

Table 1

Metabolite Ratios From Patient and Control Group

Metabolite Ratio	Patient PWM	Control PWM	2SD	Patient PGM	Control PGM	2SD	Patient Cereb. WM	Control Cereb. WM	2SD	Patient Cereb. GM	Control Cereb. GM	2SD
NAA/Cr	1.60[a]	2.05	0.90	1.44[a]	1.77	0.35	1.72[a]	2.35	0.76	1.48	1.40	0.32
Cho/Cr	1.28[c]	0.94	0.14	1.01[c]	0.68	0.09	0.95	0.92	0.33	1.56[c]	0.78	0.05
Ins/Cr	1.68[c]	0.63	0.91	0.85[c]	0.61	0.22	1.14[c]	0.60	0.41	1.53[c]	0.53	0.09
NAA/Cho	1.26[a]	2.17	1.00	1.43[b]	2.60	0.70	1.81[a]	2.57	1.03	0.95[b]	1.79	0.40

Data presented as means and 2 SD.

[a] <1 SD.

[b] <2 SD.

[c] >2 SD.

Table 2

Metabolite Integrals From Patient and Control Group

Metabolite Integral	Patient PWM	Control PWM	2SD	Patient PGM	Control PGM	2SD	Patient Cereb. WM	Control Cereb. WM	2SD	Patient Cereb. GM	Control Cereb. GM	2SD
NAA	13.9[a]	42.7	27.6	11.4[a]	45.6	7.87	16.1	18.47	7.80	12.[a]	20.1	5.13
Cr	8.65[a]	20.6	4.89	7.91[a]	25.7	8.83	9.40	7.84	1.61	8.15[a]	14.4	2.38
Cho	10.5[a]	19.4	5.67	7.99[a]	18.3	3.67	8.95	7.17	2.04	12.7	11.2	1.61
Ins	14.6	13.3	21.4	6.71[a]	17.2	7.20	10.7[b]	4.61	2.38	12.5[b]	7.67	2.43

Data presented as means and 2 SD.

[a]<2 SD.

[b]>2 SD.

Table 3

Regional Variations in FA: Mann-Whitney Test

Region	Patient		Control Group			*P*-value
	N	Mean	N	Mean	2SD	
CST	40	0.426[a]	200	0.559	0.20	<0.005
CC	7	0.716	35	0.727	0.092	0.552
OR	14	0.279[a]	70	0.532	0.128	<0.005
MCP	6	0.493[a]	30	0.556	0.112	0.016

[a]<2 SD.

CC, corpus callosum; MCP, middle cerebellar peduncle; OR, optic radiations; CST, corticospinal tract; N, number of regions of interest.

Table 4

Regional Variations in ADC (in 10-3 mm 2/sec): Mann-Whitney Test

Region	Patient		Control group			*P*-value
	N	Mean	N	Mean	2SD	
CST	40	0.956[b]	200	0.689	0.176	<0.005
CC	7	0.750[a]	35	0.689	0.076	0.014
OR	14	1.284[b]	70	0.768	0.122	<0.005
MCP	6	0.828[b]	30	0.663	0.122	<0.005

[a] >1 SD.

[b] >2 SD.

CC, corpus callosum; MCP, middle cerebellar peduncle; OR, optic radiations; CST, corticospinal tract; N, number of regions of interest.